NPL
National Physical Laboratory

Report

NPL Report ENG 5

Review of Low Force Transfer Artefact Technologies

Christopher W Jones, Richard K Leach

March 2008

National Physical Laboratory | Hampton Road | Teddington | Middlesex | United Kingdom | TW11 0LW
Switchboard 020 8977 3222 | **NPL Helpline** 020 8943 6880 | **Fax** 020 8614 0446 | **www.npl.co.uk**

Department for **Innovation, Universities** & **Skills**

Review of Low Force Transfer Artefact Technologies

Christopher W Jones, Richard K Leach
Mass and Dimensional Group
Industry and Innovation Division

Abstract

Traceable low force measurement at the micro- to nanonewton level is becoming critical to advances in nanoscale research and manufacturing. Previous attempts at low force traceability and other candidate technologies are reviewed in this report. Technologies determined to be unsuitable for immediate or further exploitation include protein manipulation and those based on quantum intermolecular forces, capillary forces and radiation pressure. Technologies highlighted for further development contain an elastic element with active displacement metrology based on the piezoelectric effect, capacitance gauges, volt balances and resonant frequency shifts. All would benefit from onboard signal processing. This report will inform the design of a complete low force calibration transfer system from the NPL Low Force Balance to most typical and many atypical force producers requiring calibration.

ISSN 1754-2987

National Physical Laboratory
Hampton Road, Teddington, Middlesex, TW11 0LW

Approved on behalf of the Managing Director, NPL
by Susan Evans, Director, Industry and Innovation Division

Contents

1 Background 1

1.1 Motivation 1

1.2 The NPL Low Force Balance 1

1.3 Design constraints 3

2 Overview of current techniques and capabilities 5

2.1 Dead weight force production 5

2.2 Elastic element methods 5

2.3 Electrostatics (volt balance) and electromagnetism (watt balance) 13

2.4 Resonance methods 15

2.5 Van der Waals and Casimir forces 18

2.6 Biochemical/protein methods 19

2.7 Fluid flow deflection and capillary forces 21

2.8 Radiation pressure 22

3 Conclusions 23

Appendix A Summary of surface interaction forces 26

References 27

1 Background

1.1 Motivation

The development of a transfer artefact to provide force traceability in the micronewton to nanonewton range is motivated by the need for low force traceability in industry. Examples of fields in which traceability is now urgently required include: atomic force microscopy and instrumented indentation; micro-electromechanical systems (MEMS) characterisation and the understanding of small force mechanisms in biochemical processes.

The National Physical Laboratory (NPL) has designed a primary low force balance capable of measuring forces in the range 10 μN to 1 nN with a 50 pN resolution. The balance, which is introduced in more detail in section 1.2, derives its traceability from quantities precisely determined from fundamental physical constants, rather than by comparison to the kilogram, a physical standard whose value may change over time.

Practicalities necessitate an artefact to transfer the force standard from the LFB to a target instrument in order to calibrate it. The purpose of this document is to identify feasible technologies that may be used to create such an artefact.

1.2 The NPL Low Force Balance

In response to a growing requirement in UK and international industry for traceable force at the micronewton level, researchers at the National Physical Laboratory devised an instrument for low force measurement in terms of voltage, capacitance and displacement, which are all traceable to high accuracy [1, 2]. The result, designed in collaboration with the Technical University of Eindhoven [3], is known as the Low Force Balance (LFB). The purpose of the LFB is to provide traceable force measurement in the range 1 nN to 10 μN. The US National Institute of Standards and Technology (NIST) have also developed a balance that operates over the same range [4] and the Physikalisch-Technische Bundesanstalt (PTB), Germany, is producing force transfer artefacts [5] and a pendulum balance [6]. The Korea Research Institute of Standards and Science (KRISS) has plans in place to construct a low force balance. Much of the effort of KRISS so far has been concerned with modelling of the motion of a flexure, the dependency of good results on parallelism and mechanisms to fine-tune the geometry of the flexure [7]. Comparisons of the LFB with the NIST instrument and a primary instrument being developed at PTB will be carried out in due course [1].

The theory of operation of the LFB centres on equation (1)

$$F = \tfrac{1}{2} V^2 \frac{\mathrm{d}C}{\mathrm{d}z} \tag{1}$$

where F is the exerted, nulled force, V is the voltage across the capacitor system, and $\mathrm{d}C/\mathrm{d}z$ is the capacitance gradient of the balance. A schematic of the balance is shown in figure 1. A vertical force applied to the platen vertically displaces the connected flexure and dielectric. This displacement, measured by a plane mirror differential interferometer [8], is used by a control system to create a deflection-nulling feedback force. The feedback force is generated by a potential difference across a system of vertically oriented capacitor plates and acts vertically on the moving dielectric vane.

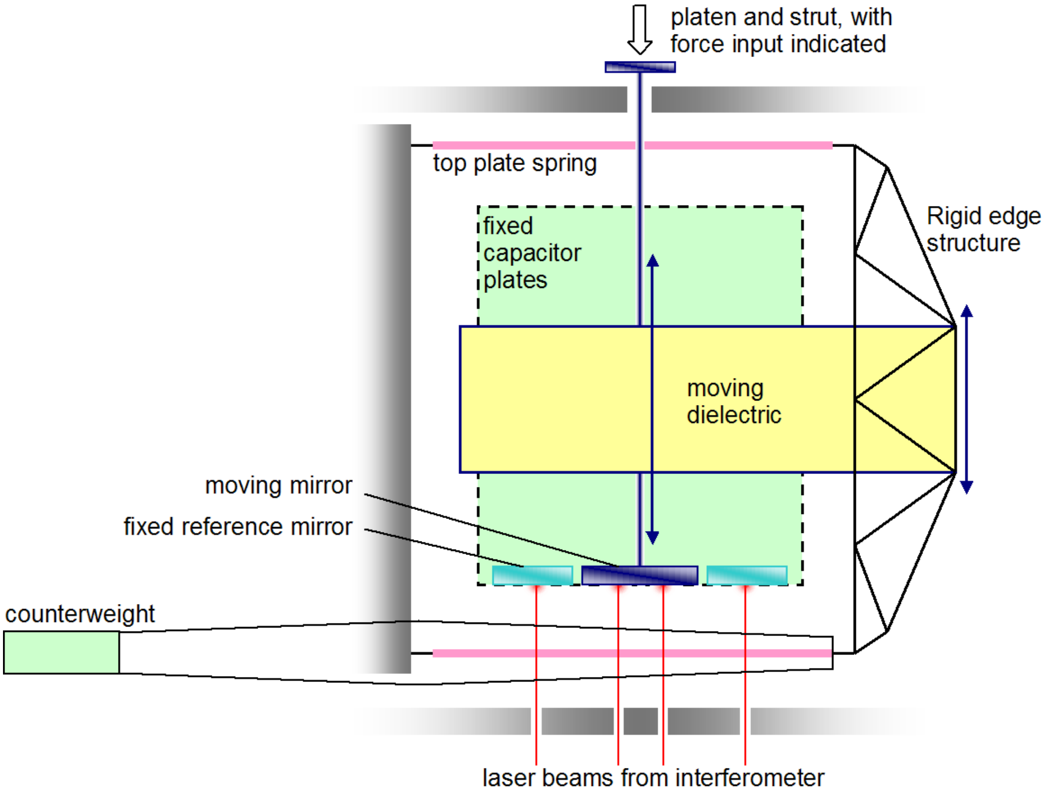

Figure 1: Schematic of NPL LFB. Relative displacement between the moving mirror and the fixed reference mirrors is determined by the interferometer and converted by a bespoke control system to a feedback voltage across the fixed capacitor plates. This voltage produces an electrostatic force on the moving dielectric vane that acts to return the balance displacement to zero.

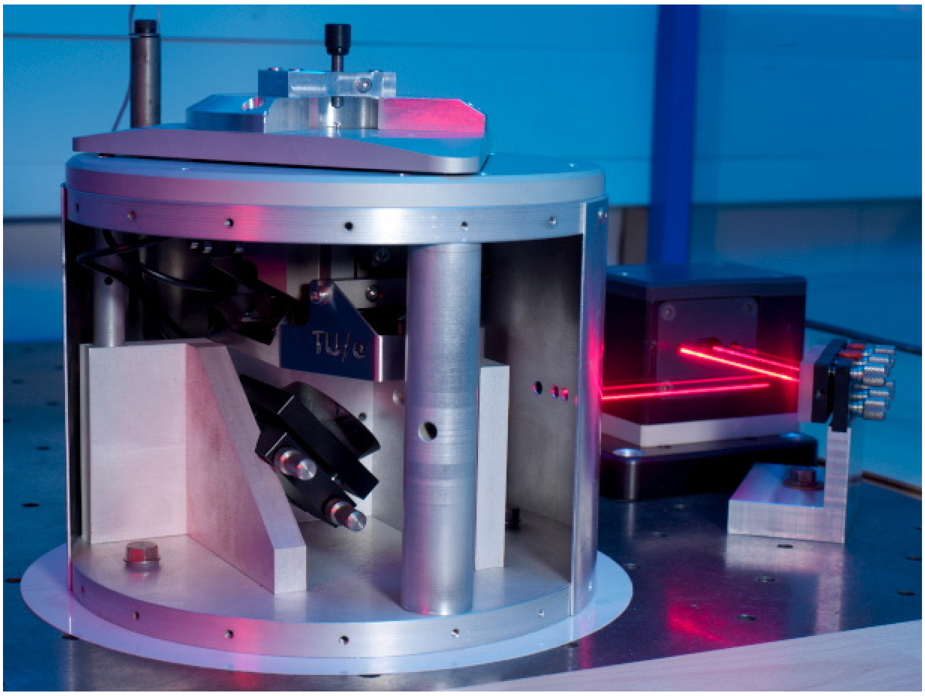

Figure 2: Photograph of the NPL LFB with a dust shield removed to show the interior. The structure inscribed with the TU/e logo forms the base of the balance mechanism shown in figure 1.

Physically the balance resembles a short cylinder of radius 100 mm and height 150 mm, with a two millimetre diameter glass rod protruding slightly from the top face centre (see figure 2). The balance currently operates in a non-airtight acoustic isolation chamber in an environmentally close-controlled laboratory (to 20 °C ± 0.1 °C and relative humidity to 45% ± 5%).

Due to the size of the balance and its associated instrumentation, its requirement for vibration isolation and its alignment sensitivity to changes in orientation, it is not possible to connect anything but small items to the balance for force measurement. From this, and from the logistics of moving each target instrument to the balance's vicinity, stems the need for a transfer artefact.

1.3 Design constraints

A successful force transfer artefact must maintain its traceability throughout the full calibration cycle of a target instrument, and the associated conditions. The key steps in the calibration cycle would consist of: calibration on the LFB; physical transport to the target instrument, calibration of the target; return transport to the LFB; and final drift testing or calibration checking on the LFB. In the ideal case the primary balance and target instrument would be a few metres apart under controlled laboratory conditions. It is more likely, however, that the calibration transfer would involve kilometres of couriered transport, with the associated levels of mechanical and thermal stress. This likelihood would suggest the use of a mechanically simple and relatively robust construction for the artefact. The artefact would ideally be small and self-contained, with the majority of processing electronics onboard, to facilitate calibration and transport as a single unit. This removes the dependence of results on users' instrumentation.

Ideally the calibration transfer facility should match the range of the LFB; it may be appropriate to divide the full 10 μN to 1 nN range between several suitable transfer technologies.

The required operational uncertainties of the transfer artefact depend on the target instrument, but in a complete transfer artefact package, uncertainties of less than 1 nN are essential, and less than 100 pN desirable, to make use of the unique force measurement range of the LFB.

The artefact is likely to require inversion with respect to gravity without losing calibration. Most target instruments probe downwards onto a sample holder; in comparison the LFB is accessible only from above. The installation of a seesaw direction changer on the balance is a possibility but would invalidate most of the unique design advantages of the balance, significantly increasing uncertainties.

The target instrument sets the limit on the physical dimensions of the artefacts. The thickness must be less than the instrument stage clearance or throat. The lateral dimensions are less constrained but must be appropriate for a stable metrology loop.

Force transfer artefacts can in principle be active, with internal force sensing, or passive, reliant on the force or displacement metrology of the target instrument.

A passive system, such as a simple elastic spring element, has no on-board metrology or force feedback. It responds in a pre-defined and pre-calibrated way to external force input. By recreating the same response using the target instrument, the calibration is in principle transferred. The method relies on the target instrument's capability; with a spring, for example, its displacement must be measured with sufficient accuracy to enable the calculation of the force acting *via* a spring constant. The position-nulled operation of the LFB introduces a further complication. A passive artefact would need to be actuated against the balance by an independent system (such as a piezoelectric element), with consequences for the stability of the metrology loop. It is often possible to characterise the stiffness of the metrology frame through direct probing with the balance, but measurement uncertainties are inevitably increased.

The advantages of a passive system, however, include the resultant simplicity of design, with advantages for modelling, the lack of internal heat or noise sources, and the elimination of costly and space-intensive metrology systems.

An active device generally registers a force against its internal scales and attempts to reproduce the force at the target instrument. Repeatability is crucial; the actual force value used is less important. An active device is usually a transducer: it produces a repeatable analogue output in response to an input force equal to the force it exerts on a target instrument. The key advantage of an active device is that it may be used directly to calibrate a passive target, such as an AFM cantilever.

A successful artefact must be able to exert a force on a passive target. As targets are generally compliant this implies a capability to push a tip into the target. There are two ways to achieve this. The first is to include a suitable powered, pushing element within the artefact. The second is to push the artefact into the target, for example for a cantilever-on-cantilever calibration. This pushing system would form part of the metrology loop and, therefore, must be stable when at rest and non-compliant. An example of such a drive would be a piezoelectric stick-slip motor.

The key challenge is in building a device of sufficient metrological performance within the size and environmental constraints. For example, the use of electrical or magnetic fields in the vicinity of the LFB and many of the intended target instruments would have to be considered carefully. Small magnetic fields of appropriate frequencies would be suitable for use near the LFB and most AFMs, but perhaps not other targets.

The artefact will be required to make contact with the LFB in a well-defined manner. The platen of the balance is currently the millimetre diameter circular top face of the glass rod, protruding from the balance body. Thus either the artefact must incorporate a tip, or one must be installed on the balance platen and characterised for the inevitable compliance at the interface. The complication is that most target instruments interact *via* their own tip, and tip-tip interactions are fraught with difficulties. A small radius sphere could form a compromise between a tip and a flat.

As stated by Pratt *et al.* [9], a successful transfer artefact would be a device with a well defined loading point, responsive to loads only along a well-defined axis, and possessing its own sensor for converting the load into a useable readout. It should be noted, however, that any guidance system would represent an alternative force path. Pratt *et al.* [9] further suggest that for the transfer artefact to be capable of use in either transfer approach, it must be compatible with both commercial AFM sensor and specimen holders, limiting the artefact volume to the typical 3.6 mm × 1.6 mm × 0.1 mm.

A starting point for NPL efforts could reflect the current NIST target of an artefact to transfer forces at the nanonewton to micronewton level with an accuracy of a few tenths of a percent [4]. This is the accuracy sought for related draft measurement standards for instrumented indentation [10] and atomic force microscopy.

2 Overview of current techniques and capabilities

2.1 Dead weight force production

The most intuitive method of force production makes use of the Earth's gravitational field acting on an object of finite mass: a dead weight. Dead weights have traditionally been, and are still used routinely, for maintaining force traceability in the millinewton to meganewton range [11]. However, below 10 µN at the higher end of the LFB scale, handling difficulties, contamination and independent testing issues lead to high relative uncertainties in weight measurement. For example, a 0.1 µg aluminium mass, equivalent to a weight of approximately 1 nN, would be a cube of side 34 µm. The trend is for the relative uncertainty to increase in inverse proportion to the decrease in mass [12], with maximum uncertainty over the LFB working range reached at 1 nN dead weight. Dead weights are, therefore, unsuitable for use as transfer artefacts, although useful for intercomparison purposes at the higher end of the force scale of the LFB.

2.2 Elastic element methods

Apart from gravitational forces from calibrated masses, the most intuitive and common technology used for calibrated force production is an elastic element with a known spring constant. The element, such as a cantilever or helical spring, is deflected by a test force. The deflection is measured, either by an external system such as an interferometer, or by an on-board MEMS device such as a piezoelectric element. With the spring constant previously determined by a traceable instrument such as an electrostatic force balance, the magnitude of the test force can be calculated. In this way a force calibration is transferred.

Several examples of elastic elements use modified AFM cantilevers, as these are of the appropriate size and elasticity, a simpler geometry than custom designs and thus more reliably modelled, and generally well understood by those working in the industry. Very thin cantilevers, the manufacture of which is now possible, have low enough spring constants to allow, in principle, force measurement at the nanonewton level.

2.2.1 Characterising cantilevers

To determine the spring constant as a function of position on a cantilever, a well known force must be applied at well defined positions along the cantilever and the resultant displacement accurately measured. The spring constant is strongly dependent on the position along the cantilever, with standard beam theory predicting an L^3 dependence, where L is the position along the cantilever from the fixed root. The cantilever would need to be brought into contact with a tip on the LFB platen and deflected such that the position of the tip on the beam is accurate, and in the interest of operational usefulness, repeatable. The same would be required when interfacing the cantilever with the target instrument. This need for accurate positioning implies that the requirement for high-magnification microscopy and high-precision initial cantilever positioning during all stages of the calibration transfer process.

The spring constants of seemingly similar elastic elements are often very different due to manufacturing imperfections and impurities in the material. Calculated estimates of spring constants based on geometry are generally inaccurate due to the combination of uncertainties. For rectangular cantilever geometry, the spring constant k is given by the following equation

$$k = \frac{Et^3 w}{4L^3} \tag{2}$$

where E is Young's modulus, t the thickness, w the width and L the length of the cantilever. The power dependence on the length and thickness dimensions and the direct contribution of the generally not accurately known Young's modulus result in relative uncertainties as high as 25% [13]. Dimensional uncertainties are compounded when a coating is applied to the cantilever, for example to enhance reflectivity [14]. For these reasons it is not currently possible to manufacture a spring with a particularly accurately predefined spring constant. Hence a great deal of effort has been applied to methods of determining the spring constant; the methods are summarised in table 1, which was adapted from [15]. Verification of the thermal method of spring constant determination has since been carried out. The precision and accuracy of the thermal method were found to be 5% and 10% respectively.

Approach	**Method, main source of uncertainty in parentheses**	**Risk of damage to tip**	**User friend-liness**	**Advantages**	**Disadvantages**
Dimensional					
Butt [16]	25%; 50% in paper (Eq. and t).	Low	High	Simple equation. Measures cantilever stiffness directly.	Not a good model, t and E needed. Requires calibration of pendulum.
Modified Neumeister and Ducker	11% (t and E).	Low	High	Simple and accurate.	t and E needed.
FEA of statically loaded triangular cantilevers [17]	10%; no attempt made at comparing with any other technique (t and E).	Low	Medium	Accuracy; computation allows both normal and lateral spring constants to be determined.	FEA programs expensive, complex, t and E needed.
FEA of oscillating composite V-shaped cantilevers [18]	6% and 25% compared with two different parallel beam approximations.	N/A	Medium	'Real' V-shaped cantilever geometry used.	Accuracy depends on uncertainty in material properties and type of parallel beam approximation used.
FEA of oscillating composite V-shaped cantilevers [19]	10% for full FEA solution.	N/A	Medium	Simple formula suggested relating the cube of the resonant frequency to the spring constant.	Applies to limited resonant frequency range. Gold coating thickness dependent.
FEA of oscillating composite V-shaped cantilevers [20]	Up to 40% for simple formula. Full FEA solution regarded as correct.	N/A	Medium	Real V-shaped geometry used.	Gold coating thickness significantly affects outcome of FEA.
Static experimental					
Static mass hanging [21] by inverting loaded cantilever	15–25% (mass attached).	High	Poor	No geometry and E data needed. Just one particle required to be added to the tip.	Accurate placement of spheres, calibrated spheres and calibrated deflection needed
Cantilever on reference cantilever [22]	10% (ref. cantilever).	Medium	Medium	Simple idea, geometry and coating independent	Difficult to set one cantilever on other accurately. Need $k_{ref} \approx k_{working}$

Approach	Method, main source of uncertainty in parentheses	Risk of damage to tip	User friend-liness	Advantages	Disadvantages
Cantilever on reference spring [23], [24]	5% (contact mechanics of working lever on ref spring).	Medium	High	Simple, potentially traceable to SI.	Contact method.
Static loading using two probes [25]	10–30% (ratio of two probe stiffnesses).	Medium	Medium	Once one of the probes is calibrated it can be used to calibrate many different probes accurately.	Best for two probes of similar stiffness. Requires accurate probe positioning.
Nano-indenter [26]	8% (nano-indenter calibration).	Low	Medium	Simple, quick.	Difficult to place indenter tip in correct position. Only for $k_z > 1$ N m^{-1}.
Dynamic experimental					
Forced oscillation/FEA [27]	15–20%; 10% compared with [28] for V-shaped levers (unloaded resonant frequency; Young's modulus).	Low	Medium	No masses need to be added, therefore, non-destructive. Just depends on unloaded resonant frequency.	Technique relies on accurate values of cantilever density and thickness.
Dynamic mass attachment [28]	15–25% (mass attached).	High	Poor	No geometry data needed.	Need accurate placement of masses. Calibrated spheres needed.
Thermal noise analysis [29]	15–20%. 20% as obtained by [30] comparing with a static loading technique. 5% as determined by [29]. Precision and accuracy of 5% and 10% respectively on a NIST-calibrated artefact [31]. (Interference from other noise sources).	Low	High once set up	Only frequency and T data needed.	Model validity unknown. Requires cantilever to be pressed against hard surface for calibration. Ignores damping effects – only for low k_z cantilevers.
Resonant freq. In air method [32]	15-20% (Reynolds no. for the fluid–cantilever system).	Low	Medium	Simple.	Only for rectangular cantilevers.

Table 1: Summary of methods for determining a cantilever spring constant (adapted from [13, 15])

The minimum force detectable by a cantilever is discussed in [33] and [34]. This minimum force relates to the cantilever dimensions; thermodynamic and Johnson noise form the fundamental limits.

The effects of temperature variation on the physical properties of an elastic element are generally significant and should not be ignored. From the ratio of stress to strain a material's Young's modulus varies as the inversion of the bulk material's relative expansion due to temperature. Use of well-known materials would facilitate calculations to compensate for expansion due to temperature, which at any rate should be well controlled. The temperature dependence of the resonant frequency of the first eigenmode of a microfabricated silicon cantilever, for example, is dominated by the variation of the Young's modulus, whereas the temperature dependence of geometrical dimensions due to thermal expansion, especially the thickness, can be neglected [35]. For piezoresistive elements, the temperature dependence of the piezoresistive coefficient and of the resistance itself will affect the sensitivity [36, 37, 38].

2.2.2 Cantilever arrays

In order to provide suitable performance across a working range, usually one spring constant is insufficient. It is common to design devices containing elements with a range of spring constants. This may be achieved in two ways with cantilever arrangements. Either an array of cantilevers with attached probes or single defined probing points is used, or one cantilever with multiple defined probing points is used. An example of the former, called an 'array of reference cantilevers', has been developed by Gates and Pratt at NIST [39] and is shown in figure 3. The arrays, microfabricated from single crystal silicon, contain cantilevers with estimated nominal spring constants in the range 0.02 N m^{-1} to 0.2 N m^{-1}. Variations in resonant frequency of less than 1% are reported for the same cantilevers across manufactured batches, as an indication of uniformity. The spring constants were verified on the NIST electrostatic force balance. These cantilever arrays are relatively cheap to produce in bulk and may lead to a disposable transfer artefact with the level of uncertainty required for AFM calibration (parts in 10^2 to 10^3) [40].

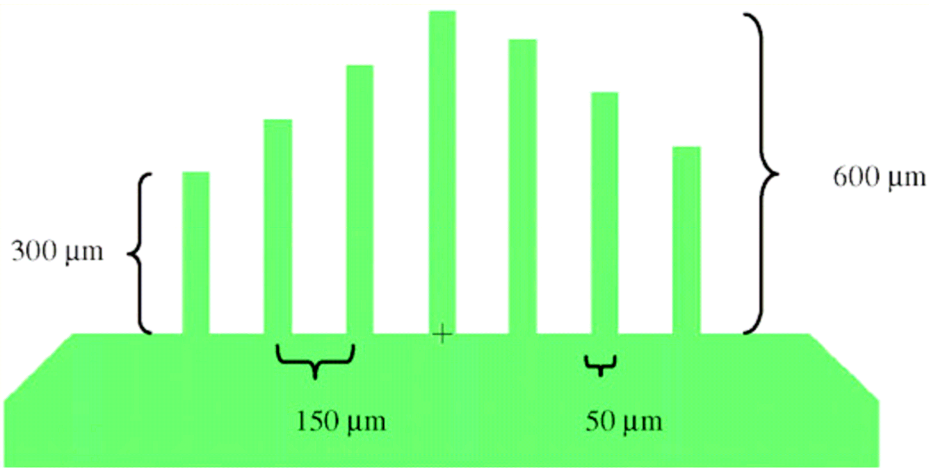

Figure 3: Experimental prototype reference cantilever array - plan view (from [39])

Cantilever arrays are already commercially available for AFM non-traceable calibration, such as an example by Veeco Probes [41], with cantilevers of width 30 µm and length 100 µm to 400 µm (see figure 4). However, their route to traceability puts a much lower ceiling on their accuracy and the uncertainties specified.

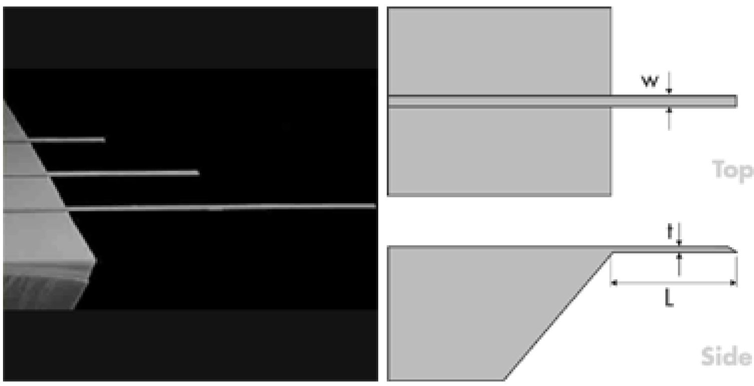

Figure 4: Commercially available AFM 'calibration' cantilevers from Veeco Probes: photograph of the three cantilevers, with quoted nominal spring constants of 0.157 N m^{-1}, 1.3 N m^{-1} and 10.4 N m^{-1} (left) and a side view of one cantilever (right) (from [41]).

As the simple devices described in this section are passive, they would require pushing into the LFB by an actuator system and some external means of measuring deflection. This second requirement is significant as it relies on the displacement metrology of the target instrument, as discussed previously. The working uncertainty of these devices is higher than active-type cantilevers, to be discussed below, and may be better calibrated by such an active-type artefact. For a primary transfer artefact, however, direct use of these examples is probably not suitable.

2.2.3 Active-type single cantilevers

The alternative to the arrays of high-quality passive cantilevers discussed above is a single cantilever with onboard deflection metrology. This metrology would add significantly to the device complexity. The device would not be a mass-produced, disposable tool; rather, it would operate as an extension of the LFB or as the second highest level of traceability for calibration laboratories in the UK – a secondary standard. These would be used to calibrate target instruments or indeed cheaper, lower accuracy, disposable transfer artefacts. Cantilevers of this active type usually are manufactured with multistage micro-fabrication [42].

One of the first examples of an AFM probe with on-board piezoresistive deflection sensing was developed by Tortonese *et al.* [42]. The device, shown in figure 5, was fabricated as a single piezoresistive strain element with pointed-tip cantilever geometry. The researchers claim a 0.01 nm (rms) vertical resolution, which is equivalent to 1 nN with a spring constant of 10 N m^{-1} for this proof of concept device.

To reduce the uncertainty of interaction position on the cantilever, and to allow operation at a range of spring constants, fiducial markings may be printed down its length. Since interactions often permanently mark the cantilever (an indentation), the interaction position may in some cases be determined by the appropriate choice of microscope after the interaction.

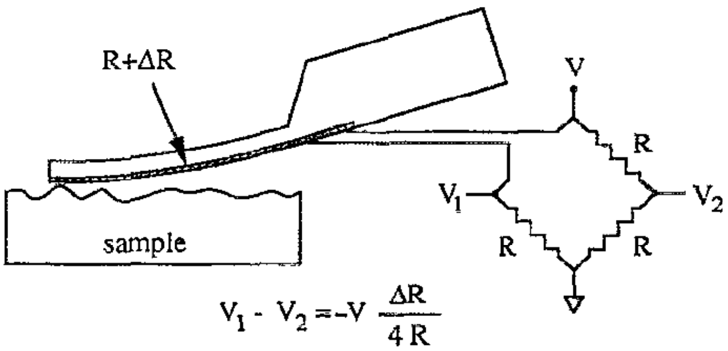

Figure 5: Tortonese *et al.*'s early piezoresistive AFM cantilever: schematic diagram of piezoresistive detection scheme (left); SEM photograph (below left) and plane view drawing (below right). Images from [42].

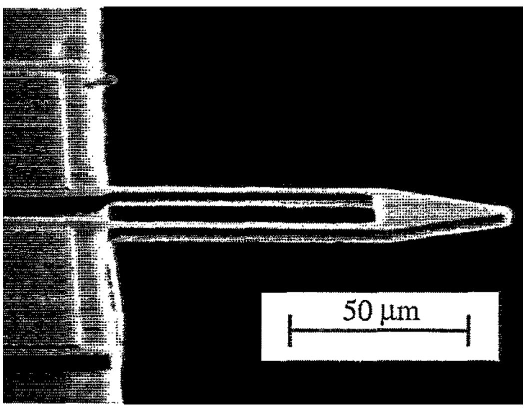

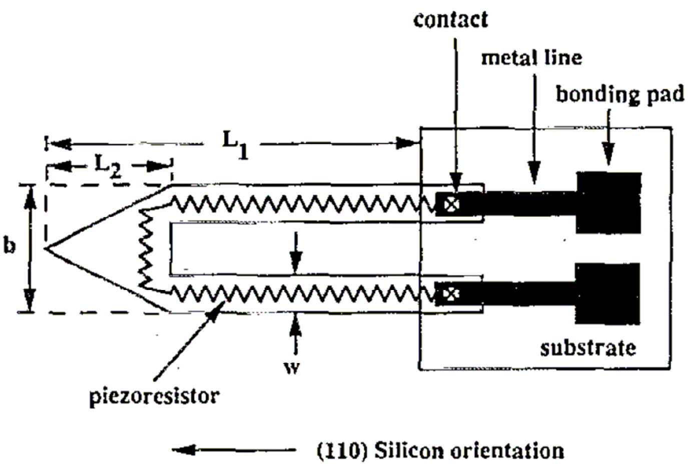

Since then, a number of piezoresistive cantilevers have been developed by several national measurement institutes. Cumpson *et al.* at NPL developed the C-MARS (cantilever microfabricated array of reference springs) device [43] as part of a set of microfabricated elastic-element devices intended for traceable AFM calibration. The relatively large cantilever (150 µm wide by 1600 µm long) is marked with fiducials that in principle allows precise alignment of the contact point for a cantilever-on-cantilever calibration. The size of the fiducials is influenced by the 100 µm × 100 µm field of view of typical AFMs. Surface piezoresistors near the base of the cantilever allow the monitoring of displacement and vibrations of the cantilever [44], if required. Detail of the device is shown in figure 6. As for many similar examples, the small mass of the cantilever renders it relatively immune to mechanical shock, and in principle could withstand transport by mail. The authors present the determination of spring constant values at the cantilever tip using Sader's method, Euler-Bernoulli theory and finite element analysis (FEA). Spring constants are also quoted for interaction at each fiducial, providing a range of 25 N m^{-1} to 0.03 N m^{-1}.

Researchers at PTB have created a slightly larger piezoresistive cantilever, of one millimetre width by a few millimetres length, for use in nanoindentation and surface texture work [44]. Commercially available AFM cantilevers with integrated strain gauges (for example Piezolever^{TM} by ThermoMicroscopes, Sunnyvale, CA) are reported to have dimensions too small for easy accurate alignment; their length and width are in the range of several hundreds and tens of micrometres, respectively. The PTB group has created both a two-leg sphere-probe example and a single-leg tip-probe example, as shown in figure 7. The prototypes, manufactured using standard silicon bulk micromachining technology, have a stiffness range of 0.66 N m^{-1} and 7.7 N m^{-1}. The authors report a highly linear relationship between the gauge output voltage and the probing force in the micronewton range.

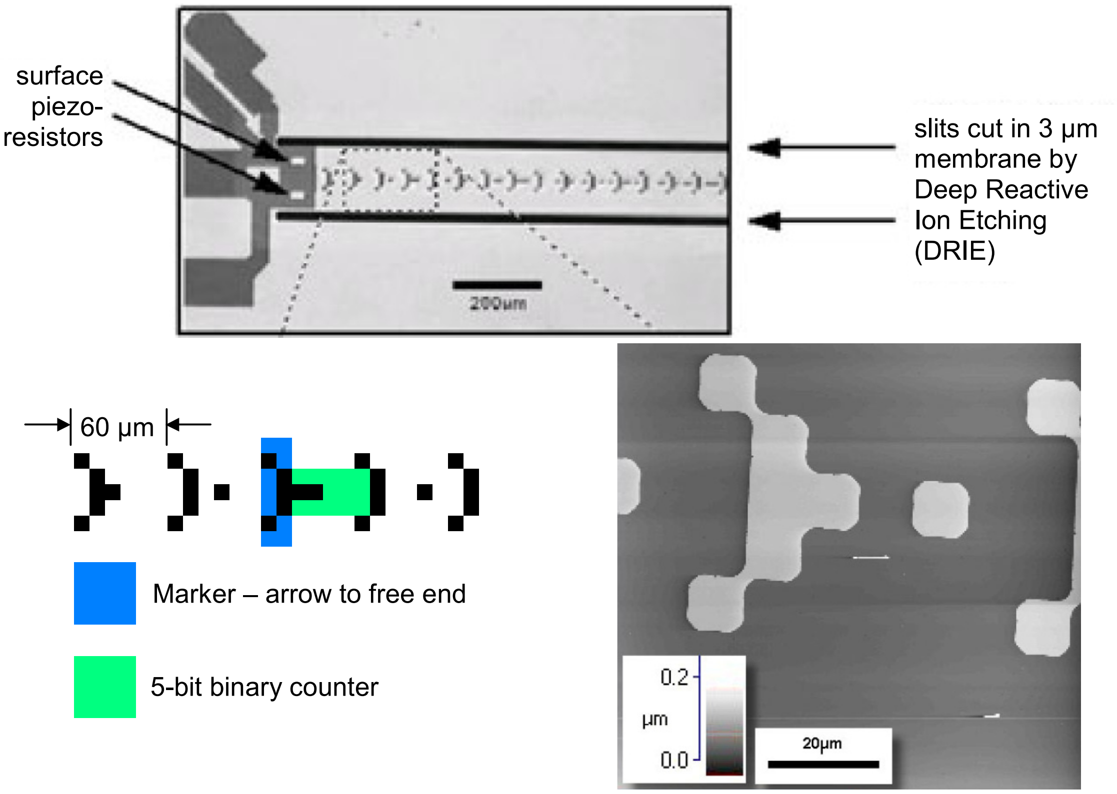

Figure 6: Images of the NPL C-MARS device, with detail of its fiducial markings; the 10 µm oxide squares form a binary numbering system along the axis of symmetry (adapted from [43]).

Most recently NIST have developed the example shown in figure 8, which has thin legs at the root to concentrate bending in this root region. Numbered fiducial markings assist in the location of balance-artefact or artefact-target interaction *via* an optical microscope [46].

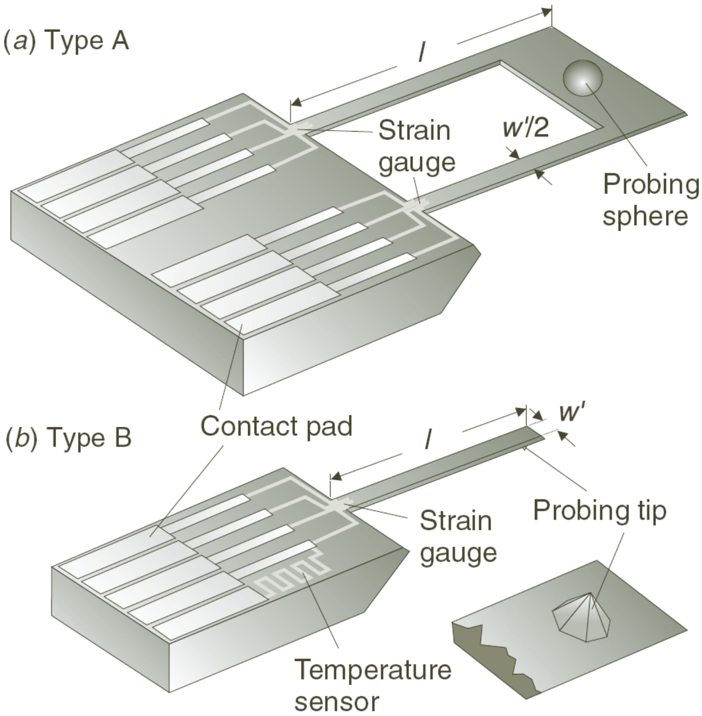

Figure 7: Types of piezoresistive silicon sensors developed at PTB: (a) two-leg cantilever with a glass sphere as probing tip; (b) single cantilever with integrated silicon tip (from [44]).

In continuous scanning mode, the probing tip of a piezoresistive cantilever, such as the NIST device, may be moved slowly down the cantilever beam, with beam deflection and external force values regularly recorded. Notches with well-defined positions show up as discontinuities in the recorded force-displacement curve, and act as a scale for accurate probe tip position determination from the data [45]. The result is a function that describes the spring constant of the transfer artefact, after probing with a low force balance. For interaction with an electrostatic force balance operating in position-nulled mode, such a device would need to be pushed into the balance tip, creating a requirement for a metrologically stable precision multi-axis stage, preferably with near-continuous positioning capability compared to the resolution of the transfer device.

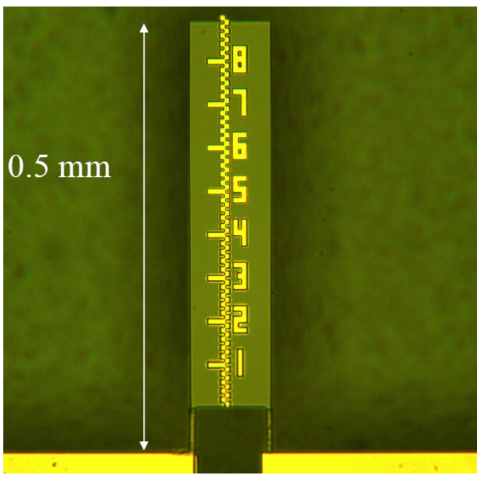

Figure 8: the NIST piezoresistive cantilever (from [40]; see also [46]).

The choice of deflection metrology depends on the working range of the transfer artefact. For the higher end of the nanonewton force range a piezoresistive element can detect displacement *via* strain. At the lower end, where displacements are smaller, capacitance methods may be used. Such on-board MEMS systems are more suited to operation in vacuum or controlled environmental conditions, as well as occupying a significantly smaller amount of valuable space. It is now possible to manufacture piezoresistive elements that require only low voltages, offer a low failure rate and onboard electronics to make the electronic output signal more user-friendly in the field. In one such example developed at Spain's Centro Nacional de Microelectrónica, very small, sensitive micro-cantilevers with integral signal-processing have been constructed on CMOS polysilicon with spring constants in the range 1.5 $mN\,m^{-1}$ to 12 $mN\,m^{-1}$ [47] (see figure 9). In another example, the development of a piezoresistive pressure sensor has been reported incorporating a MOSFET differential amplifier to improve the output signal [48].

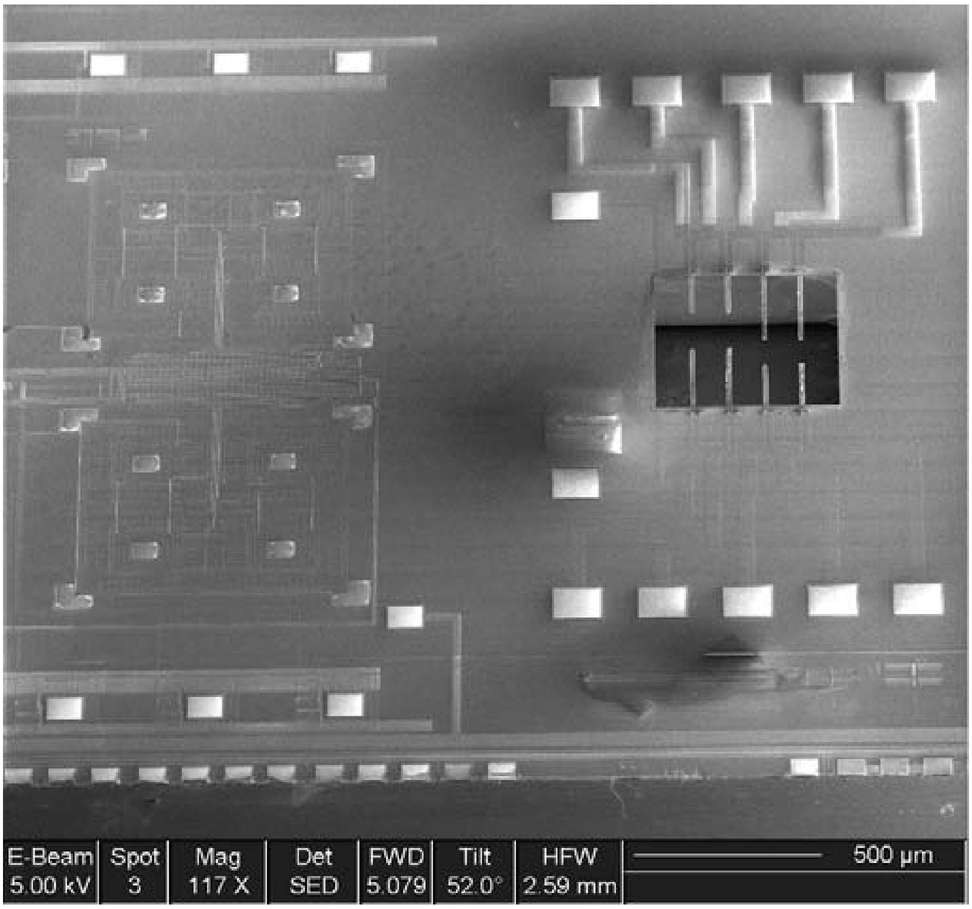

Figure 9: SEM micrograph of integrated cantilevers and CMOS circuits in an intermolecular force detection device developed at CNM-IMB, Spain (from [47]).

2.2.4 Helical springs

A different sort of elastic artefact, designed at NPL for AFM cantilever calibration, takes the form of a Microfabricated Array of (helical) Reference Springs (MARS) [23]. Twelve reflective discs are held supported above a substrate by a spring, each with a different spring constant in the range 0.16 $N\,m^{-1}$ to 11 $N\,m^{-1}$, the standard range for most contact mode AFMs (see figure 10). The low inertia springs are usefully vibration and shock resistant and in their latest form can be directly calibrated *via* their resonant frequencies and Doppler vibrometry off the mirrored discs. The authors state that the position of an interacting tip on the 160 µm discs is much less critical than with cantilevers, with the entire disc having nominally the same spring constant. This would lead to an immediate operational advantage when used in a force transfer artefact interacting with a variety of instruments. However, the design may be susceptible to parasitic deflection; this would need to be quantified. An array of tipped cantilevers of varying spring constants could offer a suitable compromise. The other challenge in the use of this device in a transfer artefact is the lack of onboard deflection metrology. An independent capacitance-based system might represent a solution.

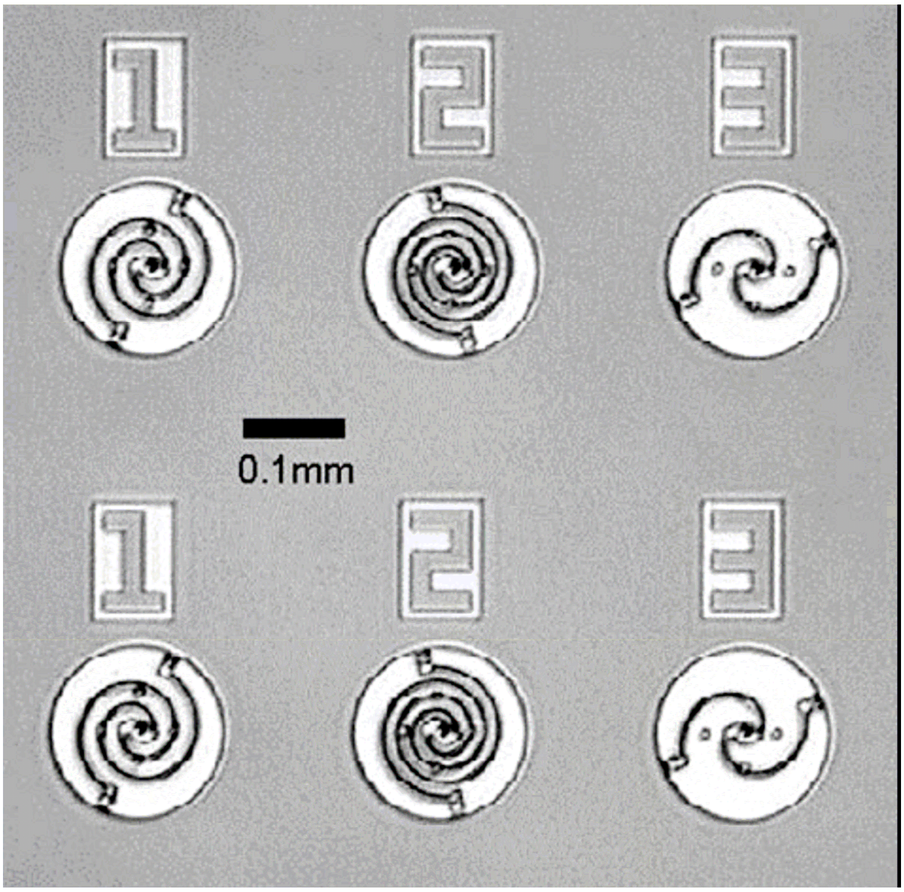

Figure 10: A MARS. Above the spiral spring is the more massive poly-crystalline silicon platform, suitable for AFM contact. A scale bar of 100 µm has been overlaid on this optical micrograph (from [23]).

The current spring constant based methods seem to offer the most direct route forward for a viable transfer artefact. A suitable version of a current technology could be housed in a suitable unit complete with a three axis translation mechanism and an independent deflection measurement system. This unit could then be kinematically mounted onto the LFB, calibrated, inverted, and installed in the target instrument. A compact fibre-fed laser interferometer could provide the deflection metrology if not achieved through MEMS technology, provided it could be made resistant to physical inversion.

2.3 Electrostatics (volt balance) and electromagnetism (watt balance)

A transfer artefact based on the volt or watt balance principles could be used as a transfer artefact, assuming its mechanism would not create unacceptable interference or cross-talk in the low force balance or the intended targets.

A possibility is to use a more compact, simplified electrostatic balance as a transfer artefact. MEMS devices are good candidates because their moving elements would have very small masses. Gravitational forces would be small improving possibilities of invertibility. Low inertia in MEMS devices lead to surprising resilience to mechanical shock.

Cumpson *et al.* at NPL have been developing novel comb-drive devices for force calibration. One example, the 'Electrical Nanobalance' device [24], is shown in figure 11. A vertical asymmetry in the fields generated in a pair of comb drives levitates a landing stage against an internal elastic element. Measurements of the driving electrical signal and resultant deflection lead to a spring constant value potentially traceable to SI. At end-use, the device becomes a passive, calibrated, elastic device requiring no electrical connections and producing no interacting fields. To convert the Nanobalance to an active device it may be possible to recalculate displacement from the capacitance across the comb-drive. The device is susceptible to stiction in the drives and to the well-known MEMS 'snap-on' effect where the moving stage catastrophically adheres to the base plate on contact due to van der Waals forces. The authors report a landing stage centre-point spring constant of 0.195 N m^{-1} ± 0.01 N m^{-1} and suitability for calibration of AFM cantilevers in the range 0.03 N m^{-1} to 1 N m^{-1}. The device, calibrated dynamically, must be operated in vacuum to avoid dust contamination of the key working elements. A similar technique is used in the same group's Lateral Electrical Nanobalance (LEN) designed to measure lateral forces such as friction in AFM [49], shown in figure 12.

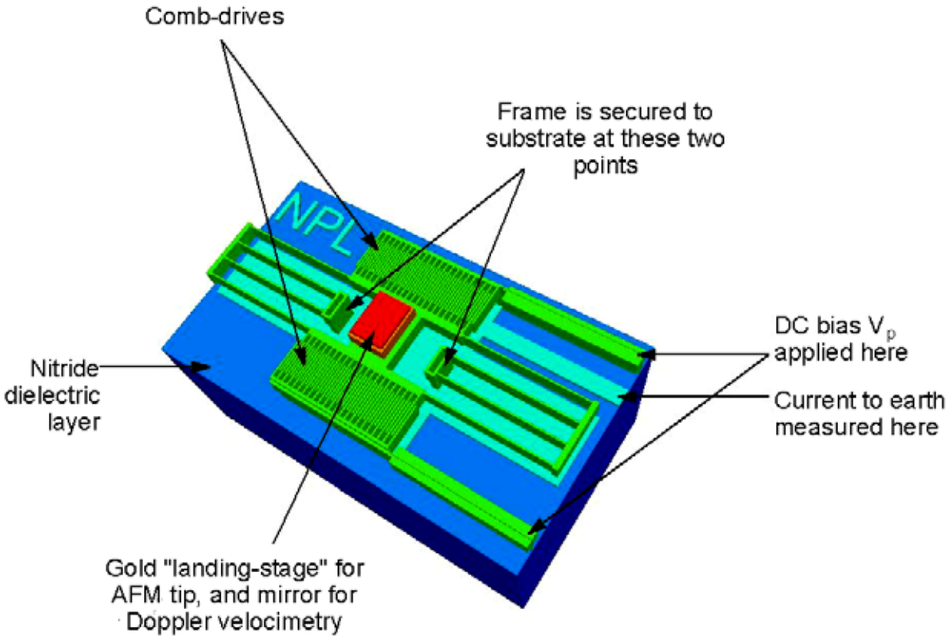

Figure 11: Computer model of the NPL electrical nanobalance device. The area shown is 980 µm × 560 µm. Dimensions perpendicular to the plane have been expanded by a factor of twenty for clarity. Taken from [24].

It may be possible, with developments in onboard signal processing, to develop a fully functioning null-servo electrostatic force balance in a MEMS package. Difficulties in altering servo parameters in a chip-implemented servo loop would point to a limited range of operation. Furthermore, a metrologically stable uni-axial flexure would be required to allow the MEMS and full size balances to each reach their set-points, adding further complexity to such a design. Two interacting servo loops would require close bandwidth matching for successful operation [40].

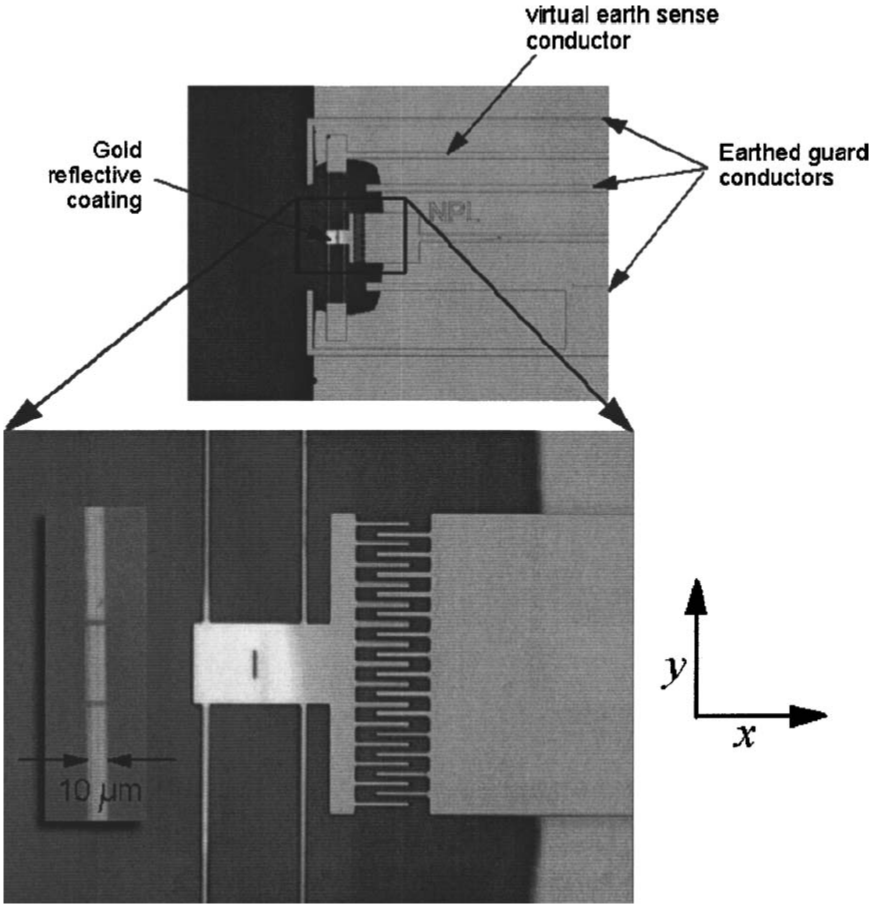

Figure 12: NPL LEN for lateral force calibration, from [49]. Inset in the expanded view is a side-on view of the 10 µm thick structure of the device.

Electromagnetism may be used for low force production or sensing *via* a voice-coil or watt balance arrangement. By using a low number of coils over a large volume, micro- to nanonewton levitating forces may be possible with milliampere to ampere coil currents. Furthermore by using a Helmholtz or Maxwell pair coil arrangement to generate a large volume of constant magnetic field, a near-constant force on the slider, set *via* the input current, may be possible. The slider would be actuated into the balance, and later the target, by a relatively imprecise and hence cheaper micro-drive, so that the slider is in the constant current zone. The current-force curve would in principle be characterised by interaction with the balance, and used in calibration transfer to the target. This is a new application of the technique successfully implemented on the NPL areal surface texture measuring instrument [50], though its cylinder air bearing system would not be appropriate for a practical low force transfer artefact. The issues associated with miniaturising a voice-coil suspension system, such that the internal friction is reduced to an insignificant level may, however, prove to be insurmountable.

2.4 Resonance methods

Changes in the tension of a stretched string can be detected *via* related changes in its resonant frequency. If a force is exerted on one of the string anchor points along the string axis, the tension in the string will decrease. For a well-characterised string the force exerted can be calculated from an accurate determination of the frequency shift. In this way a low force measurement device is created.

Force measurement *via* resonant frequency changes is an attractive approach due to the possibility for bandwidth selection. With a careful choice of working frequency through device design, the effect of noise on the measurement signal can be dramatically reduced in comparison to other methods. Operation at or near resonant modes of oscillation lowers energy requirements, in turn permitting lower power consumption and reduction of related heating effects. A lower limit to energy requirements is set by damping effects at device component boundaries, highlighted in examples below, and by intrinsic dissipation [51].

The drawback with current examples, however, is the need for optical interrogation of the resonant frequency by laser Doppler vibrometry [52]. This significantly adds to the complexity of the device. Furthermore, the published designs only transfer force in one direction, and hence cannot be used on both the LFB and the target instruments.

One apparently successful resonance force sensor is Stalder and Dürig's 'nanoguitar' [53] (see figure 13). Operating in vacuum, an SFM tip is pressed against the sample cantilever, changing the tension in the oscillating string. The beam is required to be soft compared to the string to transmit the interaction force, improving sensitivity. The setup allows micrometres of string oscillation amplitude without significant amplitude of parasitic oscillations in the connected cantilever beam. The selection of a cantilever with a lower resonant frequency than the string helped prevent such parasitic oscillations. The prototype used a carbon fibre with a diameter of 5 µm and a length of 4 mm, oscillating at 4 kHz. As string tension is decreased, force sensitivity rises but the response time drops. The force resolution is limited by thermal noise in the string oscillation. The authors report a force resolution of 2.5 nN, achieved in vacuum for a response time of 1 ms and a sensor stiffness of 160 N m^{-1}. The sensor performance was limited by a low *Q*-factor and required precise fibre tension adjustments. Vibration damping was significant because the string was glued to the cantilever. Initial tension was set by sliding one anchor relative to the other using a stick-slip mechanism. Oscillations were generated using the Lorentz force, an approach probably inappropriate for a suitable transfer artefact due to the likely interaction with the Low Force Balance. Even small ferromagnetic elements found in sample stage drives can contribute systematic force offsets on the order of a nanonewton [40].

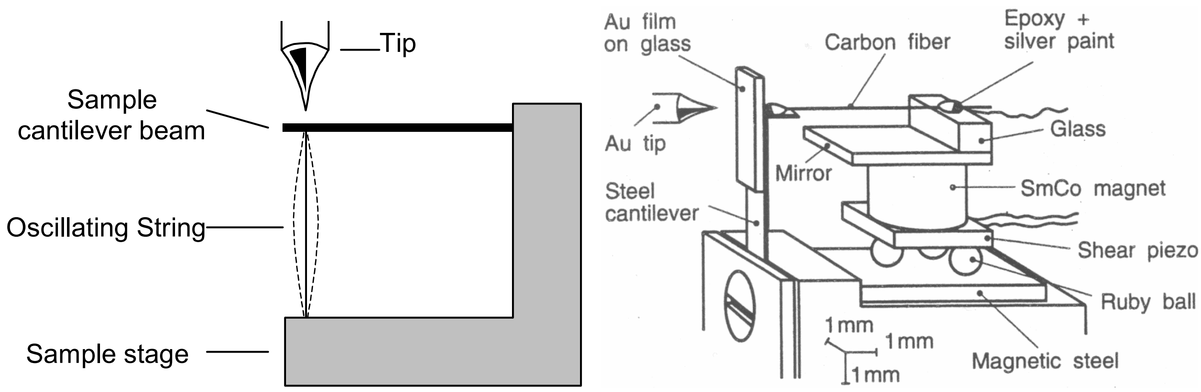

Figure 13: (left) schematic diagram of a resonance string sensor; (right) example of actual experimental set-up showing shear piezo for tension adjustment and magnet for actuation of Lorentz oscillations (from [53])

Assuming the behaviour of the cantilever beam and string can be adequately modelled and designed to allow inversion, the remaining challenge would be to suitably mount an optical detector system to record the resonant frequency, for example with a fibre laser feed. Advances in MEMS technology mean that onboard diode lasers, light guides, focussing optics and photodetectors are possible. Thus, it may well be possible to build a complete onboard vibrometer, using the Stalder and Dürig method of detecting light bypassing the oscillator. A further level of sophistication could be the use of a small Fabry-Pérot interferometer using reflected light, although returning light intensity levels from the oscillator might prove insufficient. In any case, the cost of successfully prototyping a device of such complexity may prove prohibitive for commercial exploitation.

The double-ended tuning fork concept forms an alternative high-sensitivity force sensor, and has been studied by various groups. In an example presented by Fukuzawa *et al*. [54] a vertical force acting on the sample cantilever beam changes the resonant frequency of the fork 'prong' beams (see figure 14). The beams are vibrated by an external electromagnet and the amplitude measured with a laser Doppler velocimeter. The monolithically manufactured system has an experimentally determined minimum detection force limit of 19 µN, with a theoretical value as low as 0.45 µN, which is too high for use with the LFB.

Finite element simulation of a further double-ended tuning fork example is presented in [55]. This sensor was designed to be applied as a vibratory gyro-sensor, detecting acceleration in automotive applications for example. The sensor is not directly adaptable into a transfer artefact but the presented discussion provides an insight into noise reduction (through signal subtraction), device manufacture and oscillation driving methods.

A further example resonator was constructed to allow force measurements in the presence of large force gradients (see figure 15) [56]. Such force gradients are produced, for example, by sudden conformation changes when stretching proteins with an AFM. The presented AFM sensor probe employs a piezoresistively detected, electrostatically driven resonant beam sensor oriented perpendicularly to the sample surface. The authors report a force resolution of 9 nN in a 1 kHz bandwidth in air with an oscillation amplitude of 36 nm and a resonance quality of twenty. In a 1 mtorr (133 mPa) vacuum the force resolution in the same bandwidth improves to 200 pN with a resonance quality of 450 and oscillation amplitude of 53 nm. The resolution of the detector is limited by the white noise of the piezoresistor. The piezoresistor was chosen due to the difficulties in directing light onto the oscillator in an AFM for optical vibrometry.

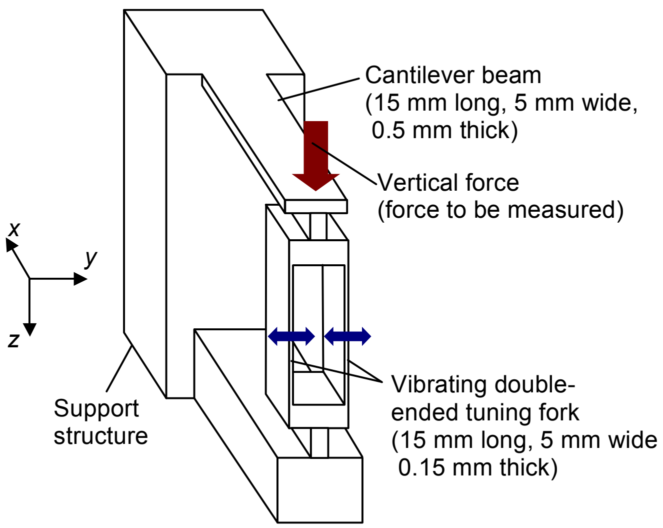

Figure 14: Schematic diagram of a double-ended tuning fork resonance force sensor (from [54]).

Currently uncertainty levels are two to three orders of magnitude too large for use in a nanonewton range, piconewton resolution transfer artefact. This level of uncertainty is perhaps a result of the larger, centimetre scale of previous examples. Since many properties scale with size, mathematical modelling may determine that by scaling down the system by a factor of one hundred may bring uncertainties down to a level permitting transfer of nanonewton forces. Furthermore, recent MEMS research may provide the solutions to challenges associated with frequency detection and device inversion can be overcome. Hence resonance methods based on the above prototypes are worthy of some further investigation.

A possible route to miniaturisation of the nanoguitar concept could exploit recent developments in carbon nanotube technology, though further innovation is required. Sazonova *et al.* describe an attempt to create a tuneable carbon nanotube electromechanical oscillator whose motion is both excited and detected using the electrostatic interaction with the gate electrode underneath the tube [57]. They highlight the advantages of the nanotube: they are made of the stiffest material known, have low densities, ultra-small cross-sections and can be defect-free. The group report that despite great promise they have as yet failed to realise a room-temperature, self-detecting nanotube oscillator due to practical difficulties. For example, the adhesion of the nanotube to the electrodes inevitably reduces the device's quality factor by several orders of magnitude. Any successful implementation is likely to require a vacuum environment, reducing its usefulness.

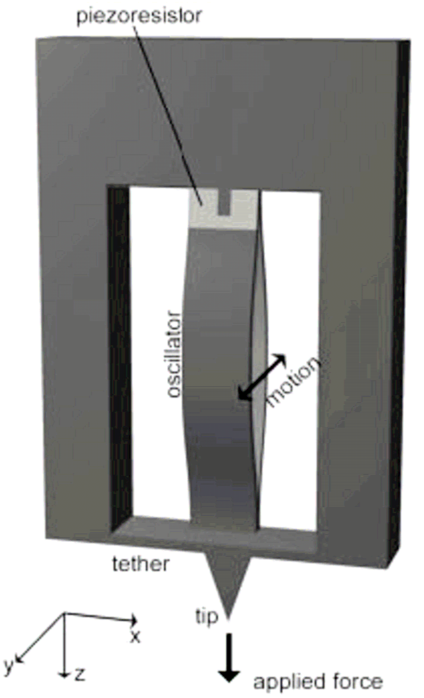

Figure 15: Illustration of resonance force sensing AFM tip presented by Harley *et al.* (from [56])

2.5 Van der Waals and Casimir forces

A manifestation of quantum effects within individual atoms, the van der Waals has been demonstrated in the nanonewton regime using MEMS-scale technology [58, 59]. This range compatibility and the force's ubiquitous nature would suggest the use of the van der Waals in a force transfer artefact. However, the force only has a useful magnitude under very small separations that are experimentally very difficult to maintain. Interacting surfaces must be very well characterised; clean, uncharged and nonmagnetic, to remove other force production mechanisms; and the operating environmental conditions must be carefully controlled. Usually operation in vacuum is required to avoid effects from particles between surfaces. Specialist equipment would also be required to measure the surface separation, and the traceability of such measurement would likely be very poor. Furthermore, traceable application of the van der

Waals interaction requires the determination of the Hamaker constant [60], which varies depending on the interacting materials, to a level of accuracy not currently available.

Considered a macroscopic equivalent of the van der Waals force, the Casimir effect is becoming increasingly important in the development of the ever-smaller, miniaturised components of emerging microtechnologies and nanotechnologies and has been investigated by various groups [61, 62, 63]. The Casimir effect is an outcome of quantum field theory. Applying boundary conditions to the quantum electromagnetic field around interacting bodies reveals a vacuum energy mismatch that manifests as a very small force. The size and direction of the Casimir force depends on interface geometry. As an example of operating range, the attractive Casimir force between two mirrors, each of area 100 mm^2, placed 1 μm apart, is approximately 100 nN. The net Casimir effect between a sphere and plate is a repulsive force. Practical experiments using the Casimir effect suffer the same requirements as van der Waals interaction experiments [64] and both would appear impractical and insufficiently understood for a transfer artefact solution compared to the more straightforward alternatives discussed elsewhere in this document.

The reader is directed in passing to research undertaken at KRISS, South Korea, to realise piconewton mechanical forces based on counting flux quanta in a cantilever mounted superconducting ring [65]. While these forces are too small for the current transfer artefact application, the work may inform the development of a piconewton regime balance system and aid the quantitative analysis of the van der Waals force.

2.6 Biochemical/protein methods

At first inspection, the stepped force trace produced when unfolding protein structures such as DNA provide a elegant and readily available source of transfer artefacts for the high-piconewton to low nanonewton range. A single protein is attached at each end to a piezoelectric translator and the force probe of the LFB or target; the former stretches the protein whilst the latter records the tension in the protein.

This topic has been extensively studied by various groups, for example [66, 67, 68]. Apart from artificial constructs, the usual choice of working protein is titin, probably the longest common protein at around 1 μm in length [69]. Well-defined force steps in the 100 pN to 300 pN range, as protein structures are unfolded in sequence, have been reported (see for example [70]) (see figure 16). To demonstrate the measurement bandwidth performance of so-called 'small' cantilevers (length of order 10 μm), Viani *et al.* [34] repeatedly stretched a titin molecule, obtaining extension-force curves as shown in figure 17.

From a metrology point of view there are significant problems associated with using protein unfolding in a transfer artefact. The mechanisms for folding and unfolding are not sufficiently understood to put confidence on the repeatability of the behaviour of a protein based 'spring'. A discussion of comparative times of refolding and spontaneous unfolding is presented in [71]. Hysteresis and hence irreversibility is common for large proteins, although not universal [72]. Clearly, one would not be able to isolate one characterised protein molecule and reuse it for each step of a calibration transfer between the LFB and a target; it would be 'lost' between disassembling the LFB-artefact interaction and assembling for the artefact-target interaction. The assumption must be made that all molecules behave alike; this is unsatisfactory for application in a high-accuracy transfer artefact.

The inconvenience of special laboratory conditions, equipment and skills required for protein handling, along with the not insignificant challenge of 'installing' a protein onto the LFB platen, would add significantly to the cost and risks for this method.

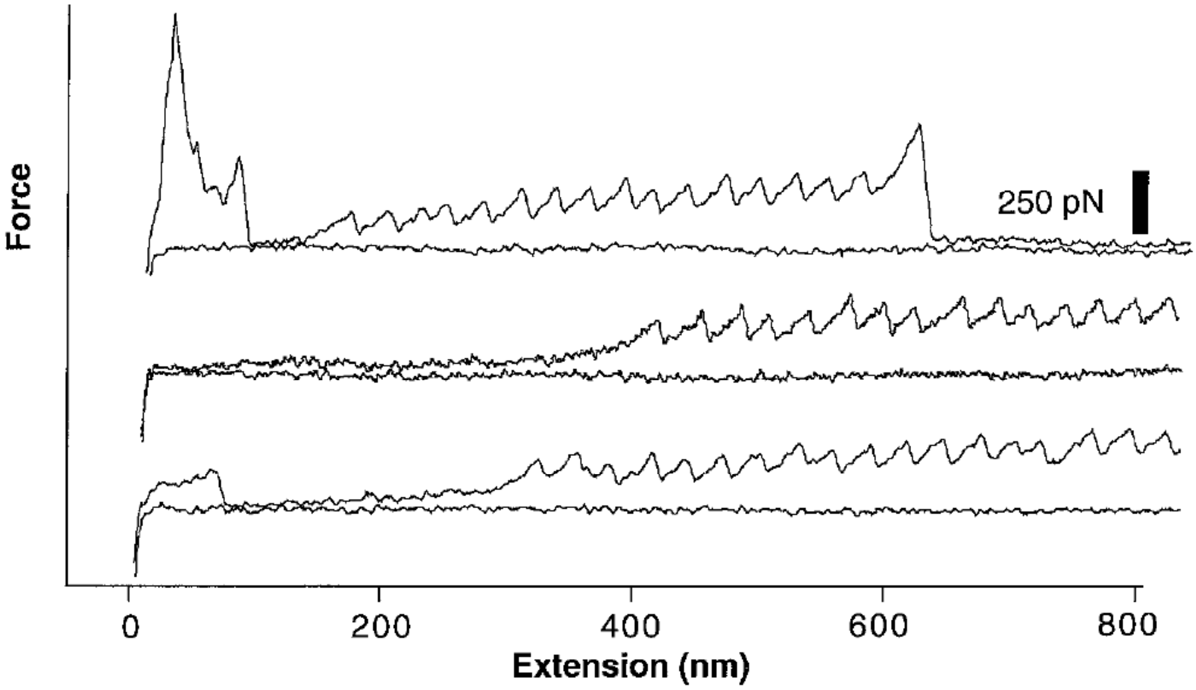

Figure 16: Extension-force curves obtained by stretching titin proteins show periodic features that are consistent with their modular construction (from [70]). Force extension curves obtained by stretching titin proteins show periodic features that are consistent with their modular construction. The extension curve in the spacer region preceding the saw-tooth is not well defined and would likely hinder traceability.

An alternative, perhaps for future consideration, is the artificial creation of simplified biochemical 'binding-site' structures on two interacting surfaces, with calculable interaction energies and hence force-separation curves. At the most basic level charge writing [73] could be used; developing further, whole artificial binding molecules could be configured on a surface, preferably in arrays for comparison.

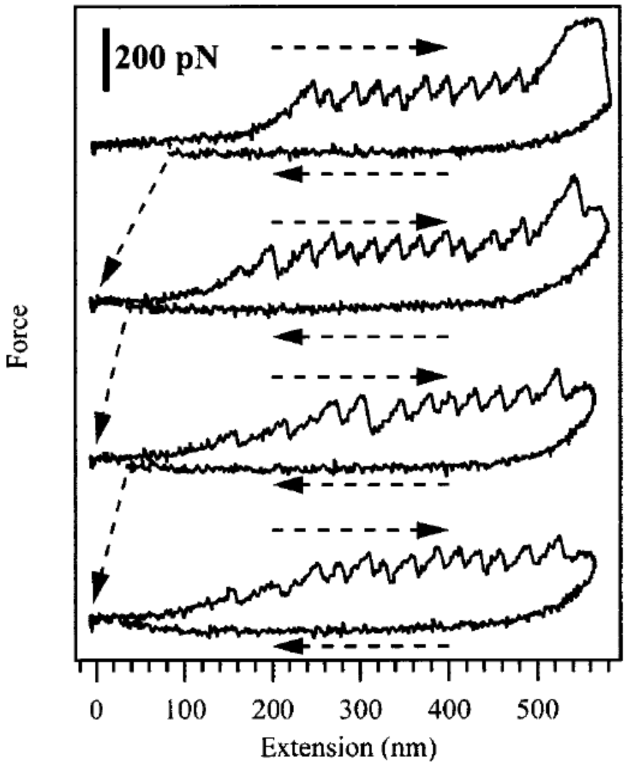

Figure 17. Four consecutive extension-force curves on a single titin molecule using a ‘small’ (length ~ 10 µm) cantilever. All extension curves were acquired at a pulling rate of 30–39 mm s^{-1}, which is an order of magnitude faster than previously performed with conventional cantilevers. System was left at rest for thirty seconds between pulls to allow protein to refold (from [34]).

2.7 Fluid flow deflection and capillary forces

Nanonewton forces may be generated by directing a suitable flow of a fluid at a target that deflects that fluid. Force is generated from the change in fluid momentum. To generate sufficiently small forces for use here, the fluid would either need to be very low in density (and hence a gas) or flowing at an extremely low rate.

Actuation of an AFM cantilever in a fluid by an acoustic transducer at radio frequencies has been more successfully demonstrated [74] but as a dynamic method is not suitable for this application.

Force production by fluid flow is likely to be very noisy, extremely hard to set up, and will produce poor repeatability. The flow of fluid could have implication for the proper operation of the low force balance and any target instrument, particularly due to thermal disturbance.

Surface tension in liquids can produce forces at the nanonewton scale (see for example [75]). Indeed the capillary forces generated from condensate forming between a probe tip and sample surface in atmosphere are a common nuisance for the experimenter. Even a monolayer of water molecules can cause significant capillary attraction between hydrophilic surfaces [58]. Hysteresis and balance servo-lock disturbance due to force-displacement discontinuities increase uncertainties in force measurement and can physically damage smaller probes. The relative size of these forces would suggest good candidacy for use in a transfer artefact. However, the difficulties in establishing the contact surface geometries and separation and hence the liquid surface shape, combined with fluid property changes due to humidity and local surface chemistry, makes force prediction and traceability extremely difficult. These methods are, therefore, unsuitable for use in a force transfer artefact. Fortunately provided capillary force issues during contact cycling can be overcome, for example by suitable servo loop tuning, capillary forces do not contribute once contact is made.

2.8 Radiation pressure

The optical pressure exerted by a focussed laser beam is currently under consideration for verification of the lower end of the LFB's force range, adapting similar examples (such as Feat *et al*. 2005). This technique could be adapted for calibration transfer purposes at the lower end of the LFB operating force range. A medium power laser would be directed onto the end of the balance platen, to which a very high reflectivity (> 99.99%) mirror is attached, of suitable size to intercept most of the laser light. From any standard text (for example [76]) the radiation pressure p_{rad} on a surface, reflecting fraction α of the incoming radiation of intensity I, with speed of light c, is given by

$$p_{\text{rad}} = \frac{(1+\alpha)I}{c}\,. \tag{3}$$

In the ideal case, the force F_{rad} generated on a perfectly reflective (α = 1) platen by a perpendicularly impinging laser beam of power W is given in by

$$F_{\text{rad}} = \frac{2W}{c}\,. \tag{4}$$

This simple model indicates that, in the best case, a nanonewton of force would be generated by 150 mW of input optical power. Care would need to be taken to eliminate spurious radiometer effects, which would need to be traded off with lower heat dissipation when deciding on the use of a vacuum for operation. Some noise will originate from the effect of particles boiling off the mirror. The design of the NPL LFB combined with operation in position-nulled mode is such that thermal expansion in the vicinity of the platen would have a negligible effect on the measured force. Furthermore, with a high-reflectivity mirror in place the transmitted power would be of the order of a milliwatt or less, acceptable provided exposure times are kept short.

3 Conclusions

In this report we have reviewed a number of candidate technologies for transfer artefacts against the specific requirements of both target instruments and the NPL LFB. Constraints such as possible uncertainties, ease of development, risk and prior experience of other groups have been considered. The findings are summarised in table 2.

Technology	Advantages	Disadvantages
Deadweight forces	Straightforward use. Need only a reliable lifting mechanism and correct material choice. No development.	Handling uncertainties; used as low force balance verification route.
Elastic element methods	Simple, well-established technology. Focus on ensuring traceability in a proven technology. Robust.	Integration of onboard deflection metrology. Dependence on position of interaction.
Electrostatics, and electromagnetism	MEMS watt and volt balances currently available and hence development relatively cheap and quick.	Integration of onboard deflection metrology without compromising primary mechanism. Crosstalk with balance.
Resonance methods	Promises lower relative uncertainties. Development of poorly represented technology would offer market an alternative.	Practical issues: bandwidth selection, low *Q*s, miniaturisation and absolute uncertainties. Risky development. Prototype iterations could prove costly.
Van der Waals and Casimir effect	Harnessing ubiquitous forces.	Extreme short-range interaction, implying less robust artefact. Dependence on interaction geometry. Hamaker constant determination.
Biochemical and protein manipulation	Possibility of intrinsic and hence highly repeatable force calibration.	Collaboration required due to new skills. Better for smaller forces (future work).
Fluid flow and capillary forces	Capillary forces always present and must be understood anyway.	Fluid flow totally unsatisfactory. High uncertainties in capillary methods due to, e.g. humidity dependence. Required level of traceability highly unlikely.
Radiation pressure	Simple experimental setup in principle.	High-power laser (heating, safety), used as low force balance verification route.

Table 2: Summary of findings

It is clear that to obtain the desired transfer artefact performance in terms of size, robustness and portability, the artefact system should take the form of a MEMS device. NPL has considerable prior experience in MEMS device production and can outsource the final device design and manufacture. Recently reported examples of devices with onboard electronics suggest an advantage in a complete self-contained design with a simple voltage analogue signal output. This would remove the dependence of the artefact performance on the connected hardware and the possible need to ship that hardware with the artefact. However, the initial cost of prototyping such a design and the manufacturing cost (and hence a non-disposable nature) should not be underestimated.

In summary the following are key requirements for a successful transfer artefact. The artefact must interface with the NPL LFB pan, with the help of a metrologically stable adjustable mounting and viewing system if necessary. Such a system would probably be based on a low-specification AFM for simplicity. The artefact should also interface with other electrostatic force balances worldwide, in particular the NIST EFB, to facilitate comparison. The current iteration of the NIST EFB is configured with stable translation stages and an optical microscope viewing system compatible with AFM cantilever format devices. As the NIST EFB operates in an evacuated chamber, vacuum compatibility is desirable. This places a limit on the choice of materials. It should be noted that for most applications, satisfactory operation in standard atmosphere would be required.

The device must maintain calibration after inversion with respect to gravity due to the different approach directions of the LFB and targets such as AFMs. This points again to micro-scale devices where gravitational effects are very small.

This review has shown that a number of apparently successful calibration transfer systems exist performing at the higher end of the LFB force range. A successful artefact would cover the operating range of the LFB but would focus on the lower end of its performance. Uncertainties of less than 1 nN are essential, and less than 100 pN desirable, to make best use of the force range of the LFB.

To ensure the calibration transfer ability it is essential that the artefact is self-contained. If external metrology is required, this must form part of the artefact system, and would need to be present when calibrating a target instrument. In the case of artefacts based on elastic elements, this points strongly to the use of a MEMS-based displacement sensor, such as the piezoresistive elements or capacitor arrangements used on a number of examples presented in this report.

Several candidate technologies can be immediately dismissed on closer inspection. The extreme short ranges and non-linear effects, combined with exacting geometrical tolerances and poorly known material constants, mean that atomic and quantum effects will not yield a traceable transfer artefact. The uncertainties associated with fluid flow methods are simply too high. Surface tension methods introduce the complications of surface contamination, place a high dependency on atmospheric contamination and humidity and disallow the option of vacuum operation, required for international comparison and some target applications.

Radiation pressure is to be used in the low-range performance verification of the balance and could be used as an independent method for calibration transfer. Furthermore the high-power laser set-up and associated safety mechanisms are not particularly portable.

Biochemical methods, such as protein unfolding, will become the focus of future work as the calibrated force scale is reduced further. This field will hopefully lead to intrinsic force standards: repeatable conformation changes with fixed force input requirements that need only be characterised traceable to SI. However, for a force transfer artefact in the 10 μN to 1 nN range, biochemical methods are not the best choice.

The remaining methods are based on elastic elements, with added piezoresistive, resonance or electrostatic-based metrology. These are all well represented in reported research, although the focus has remained mostly on proof of operating principle and optimisation of micro-fabrication techniques and not on the demonstration of traceability. Furthermore, the key will be to make a design as simple as possible, to reduce costs and increase confidence in the underlying metrology.

Previous research has often emphasised the transfer of a spring constant calibration, not a force; whilst of use to the AFM field this approach is of little use in other applications. To ensure wider usefulness of the transfer artefact design, deflection metrology of the chosen transfer artefact should be self-contained, so for simple deflected springs an onboard sensor for deflection measurement would be required. A piezoresistive element would be a good choice, but as this has been the choice of most other groups it may be preferable to develop a transfer artefact based on a semi-independent technology for increased end-user confidence following inter-lab comparisons. The quickest route to force traceability would be to design an interface support to hold the piezoresistive cantilevers from NPL, NIST or PTB against the LFB platen. The support would incorporate a micrometer-scale *xyz* positioning system that is metrologically stable when at rest. The LFB platen would require an attached tip to interface with the cantilevers.

An alternative option is some form of MEMS electrostatic balance, building on work already carried out at NPL. A comb-drive would not only provide an approximately linear displacement-dependent output, but also a feedback force, depending on the mode of operation. Assuming the output fields of the full-size electrostatic primary instrument do not affect such a MEMS balance, this technology remains a valid option.

The final area for possible further development is in utilising the change in resonance with tension of a resonating elastic element. Previously one major drawback for this method was the requirement for external optical interrogation of oscillation frequency, such as a laser Doppler vibrometry system, reducing the system portability. With the advances in MEMS technology, however, it may be possible to implement an onboard frequency detection system with a simple voltage analogue output. With considerable further design work to reduce the scale, and uncertainties, of the technology, and in-depth consideration of external force interface, the technology may become suitable for use in a novel transfer artefact. However, the cost of this work may become prohibitive.

Following the discussions herein, development of a transfer artefact system based on incremental modifications of existing elastic element designs is recommended. Onboard electronics shall measure and process displacement and output a suitably ranged voltage analogue for ease of use in the field. Displacement metrology may be achieved electrostatically, *via* a piezoresistive element, or possible *via* change in resonance of a connected oscillator.

Acknowledgements

This work was funded by the DIUS (formerly DTI) National Measurement System Programme for Engineering Measurement 2005–2008. Thanks are due to Dr Jon Pratt (NIST, USA), Prof Derek Chetwynd (University of Warwick) and, amongst others at NPL, David Flack, for their respective generous contributions to this report and the NPL low force facility.

Appendix A Summary of surface interaction forces

A full derivation of the surface interaction forces significant at the MEMS scale is beyond the scope of this document, and indeed has been presented by various groups previously. Nevertheless the basic force separation dependencies are worthy of consideration by the reader and a selection are presented in table 3. Equations obtained from referenced works have, where necessary, been adapted to use common nomenclature. To simplify comparison, the interaction of a sphere and flat plate is considered where possible. Since the tips of most probes can be adequately modelled as a (hemi-) sphere, this is a suitable approach. The sphere-plate separation is assumed to be much less than the sphere radius. Figure 18 is a comparative plot using typical values for the given parameters.

Interaction	Equation
Electrostatic	$F = -\varepsilon_0 U^2 \pi R^2 / D^2$ [based on 77]
Capillary	$F = 4\pi\gamma R\left(1 - \frac{h-2e}{2r}\right)u(-h+L)$ [77, 78].
Van der Waals	$F = -\frac{HR}{6D^2}$ for non-retarded, attractive forces [79]
Casimir effect	$F = -\frac{R\pi^3\hbar c}{360D^3}$ [61]

Table 3: Summary of surface interaction force equations. In these equations *F* is a force component, *U* the work function difference between the materials, *D* the sphere-flat separation, γ the free surface energies at state boundaries, *H* the Hamaker constant and θ the contact angle of in-interface liquid on the opposing solid surfaces. In the capillary force the step function *u*(.) describes the breaking separation; *e* is the liquid layer thickness and *r* the radius of meniscus curvature in the gap.

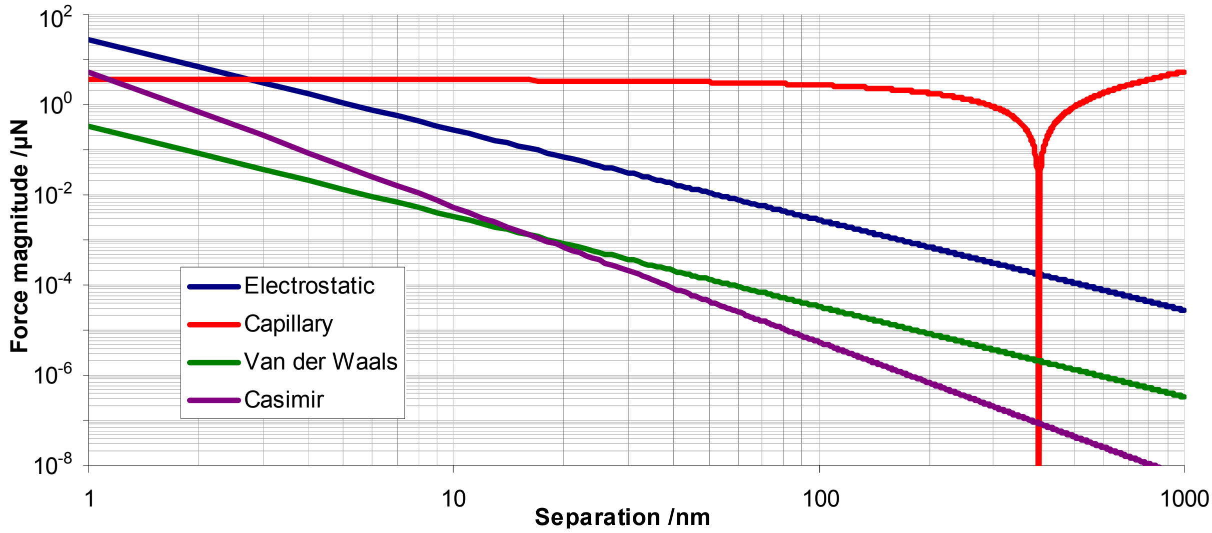

Figure 18: Comparative plot of described surface interaction forces, based on the following values: $R = 2$ μm; $U = 0.5$ V; $\gamma = 72$ mJ m^{-2}; $H = 10^{-18}$ J; $e = r = 100$ nm. Physical constants take their standard values: $\varepsilon_0 = 8.854 \times 10^{-12}$ C^2 N^{-1} m^{-2}; $\hbar = 1.055 \times 10^{-34}$ m^2 kg s^{-1} and $c = 3 \times 10^8$ m s^{-1}.

References

[1] Leach R K, Oldfield S, Georgakopoulos D 2006 Traceable nanonewton force measurement at the National Physical Laboratory, UK *Proc. 6th euspen Int. Conf., Baden, Austria, 28th May – 1st June* 414–417

[2] Leach R K, Oldfield S, Awan S, Blackburn J, Williams J M 2004 Design of a bi-directional electrostatic actuator for realising nanonewton to micronewton forces *NPL Report* **DEPC-EM-001** 1–32

[3] Henselmans R, Rosielle N, Cacace L, Kappelhof P, Klinkhamer F, Spierdijk H 2004 *Low force measurement facility: mechanical design report* (Technical University of Eindhoven)

[4] Pratt J R, Smith D T, Newell D B, Kramar J A, Whitenton E 2004 Progress toward Système International d'Unités traceable force metrology for nanomechanics *J. Mat. Res.* **19** 366–379

[5] Frühauf J, Gaertner E, Brand U, Doering L 2004 Silicon springs for the calibration of the force of hardness testing instruments and tactile profilometers *Proc. 4th euspen Int. Conf., Glasgow, UK, 31st May – 2nd June* 362–363

[6] Nesterov V 2007 Facility and methods for the measurement of micro and nano forces in the range below 10^{-5} N with a resolution of 10^{-12} N (development concept) *Meas. Sci. Technol.* **18** 360-366

[7] Choi I-M, Kim M-S, Woo S-Y, Kim SH 2004 Parallelism error analysis and compensation for micro-force measurement *Meas. Sci. Technol.* **15** 237–243

[8] Downs M J, Nunn J W 1998 Verification of the subnanometric capability of an NPL plane mirror differential interferometer with a capacitance probe *Meas. Sci. Technol.* **9** 1437–1440

[9] Pratt J R, Smith D T, Kramar J A, Newell D B 2003 Microforce and instrumented indentation research at the National Institute of Standards and Technology, Gaithersburg, MD *Proc. 4th Int. Symp. MEMS and Nanotech., Charlotte, North Carolina, USA* 299–306

[10] ISO group TC 164/SC 3/WG 1 and ASTM E28.06.11, Metallic Materials—Instrumented Indentation Test for Hardness and Materials Parameters, ISO 14577-1, 2 and 3 (International Organization for Standardization, 2002)

[11] Leach R, Chetwynd D, Blunt L, Haycocks J, Harris P, Jackson K, Oldfield S, Reilly S 2006 Recent advances in traceable nanoscale dimension and force metrology in the UK *Meas. Sci. Technol.* **17** 467–476

[12] Jabbour Z L, Yaniv S L 2001 The kilogram and the measurements of mass and force *J. Res. NIST* **106** 25–46

[13] Clifford C A, Seah M P 2005 The determination of atomic force microscope cantilever spring constants via dimensional methods for nanomechanical analysis *Nanotechnology* **18** 1666–1680

[14] Shaw G A, Kramar J, Pratt J 2007 SI-traceable spring constant calibration of microfabricated cantilevers for small force measurement *Exp. Mech.* **47** 143–151

[15] Burnham N A, Chen X, Hodges C S, Matei G A, Thoreson E J, Roberts C J, Davies M C, Tendler S J B 2003 Comparison of calibration methods for atomic-force microscopy cantilevers *Nanotechnology* **14** 1–6

[16] Butt H-J, Siedle P, Seifert K, Fendler K, Seeger T, Bamberg E, Weisenhorn A L, Goldie K, Engle A 1993 Scan speed limit in atomic force microscopy *J. Microsc.* **169** 75–84

[17] Neumeister J M, Ducker W A 1994 Lateral, normal, and longitudinal spring constants of atomic force microscopy cantilevers *Rev. Sci. Instrum.* **65** 2527–2531

[18] Hazel J L, Tsukruk V V 1996 Quantitative force measurements in SPM: vertical and torsional spring constants for V-shaped cantilevers *Polym. Prepr.* **37** 567–568

[19] Hazel J L, Tsukruk V V 1998 Friction force microscopy measurements: normal and torsional spring constants for V-shaped cantilevers *J. Tribol.* **120** 814–819

[20] Hazel J L, Tsukruk V V 1999 Spring constants of composite ceramic/gold cantilevers for scanning probe microscopy *Thin Solid Films* **339** 249–257

[21] Senden T J, Ducker W A 1994 Experimental determination of spring constants in atomic force microscopy *Langmuir* **10** 1003–1004

[22] Tortonese M, Kirk M 1997 Characterization of application specific probes for SPMs *Proc. SPIE* **3009** 53–60

[23] Cumpson P J, Hedley J, Zhdan, P 2003 Accurate force measurement in the atomic force microscope: a microfabricated array of reference springs for easy cantilever calibration *Nanotechnology* **14** 918–924

[24] Cumpson P J, Hedley J 2003 Accurate analytical measurements in the atomic force microscope: a microfabricated spring constant standard potentially traceable to the SI *Nanotechnology* **14** 1279–1288

[25] Gibson C T, Watson G S, Myhra S 1996 Determination of the spring constants of probes for force microscopy/spectroscopy *Nanotechnology* **7** 259–262

[26] Holbery J D, Eden V L, Sarikaya M, Fisher R M 2000 Experimental determination of scanning probe microscope cantilever spring constants utilizing a nanoindentation apparatus *Rev. Sci. Instrum.* **71** 3769–3776

[27] Sader J E, Larson I, Mulvaney P, White L R 1995 Method for the calibration of atomic force microscope cantilevers *Rev. Sci. Instrum.* **66** 3789–3798

[28] Cleveland J P, Manne S, Bocek D, Hansma P K 1993 A nondestructive method for determining the spring constant of cantilevers for scanning force microscopy *Rev. Sci. Instrum.* **64** 403–405

[29] Hutter J L, Bechhoefer J 1993 Calibration of atomic-force microscope tips *Rev. Sci. Instrum.* **64** 1868–1873

[30] Svoboda K, Block S M 1994 Biological applications of optical forces *Annu. Rev. Biophys. Biomol. Struct.* **23** 247–285

[31] Matei G A, Thoreson E J, Pratt J R, Newell D B, Burnham N A 2006 Precision and accuracy of thermal calibration of atomic force microscopy cantilevers *Rev. Sci. Instr.* **77** 083703

[32] Sader J E, Chon J W M, Mulvaney P 1999 Calibration of rectangular atomic force microscope cantilevers *Rev. Sci. Instrum.* **70** 3967–3969

[33] Martin Y, Williams C C, Wickramasinghe H K 1987 Atomic force microscope-force mapping and profiling on a sub 100-Å scale *J. Appl. Phys.* **61** 4123–4129

[34] Viani M B, Schäffer T E, Chand A, Rief M, Gaub H E, Hansma P K 1999 Small cantilevers for force spectroscopy of single molecules *J. Appl. Phys.* **86** 2258–2262

[35] Gysin U, Rast S, Ruff P, Meyer E, Lee D W, Vettiger P, Gerber C 2004 Temperature dependence of the force sensitivity of silicon cantilevers *Phys. Rev. B* **69** 045403

[36] Willemin M, Rossel C, Brugger J, Despont M H, Rothuizen H, Vettiger P, Hofer J, Keller H 1998 Piezoresistive cantilever designed for torque magnetometry *J. Appl. Phys.* **83** 1163-1170

[37] Rossel C, Bauer P, Zech D, Hofer J, Willemin M, Keller H 1996 Active microlevers as miniature torque magnetometers *J. Appl. Phys.* **79** 8166–8173

[38] Kanda Y 1991 Piezoresistance effect of silicon *Sens. Actuators A* **28** 83–91

[39] Gates R S, Pratt J R 2006 Prototype cantilevers for SI-traceable nanonewton force calibration *Meas. Sci. Technol.* **17** 2852–2860

[40] Pratt J R 2007 Private communication

[41] Veeco Probes 'CLFC - Force Calibration Cantilevers' product specification, retrieved from https://www.veecoprobes.com/probe_detail.asp?ClassID=9 on 25th July 2007

[42] Tortonese M, Barrett R C, Quate C F 1993 Atomic resolution with an atomic force microscope using piezoresistive detection *Appl. Phys. Lett.* **62** 834–836

[43] Cumpson P J, Clifford C A, Hedley J 2004 Quantitative analytical atomic force microscopy: a cantilever reference device for easy and accurate AFM spring-constant calibration *Meas. Sci. Technol.* **15** 1337–1346

[44] Behrens I, Doering L, Peiner E 2003 Piezoresistive cantilever as portable micro force calibration standard *J. Micromech. Microeng.* **13** S171–S177

[45] Doering L, Frühauf J, Brand U 2002 Micro force transfer standards *Joint Int. conf. IMEKO TC3/TC5/TC20, Proc. Int. Conf. On Force, Mass, Torque, Hardness and Civil Engineering Metrology in the Age of Globalisation, Celle, Germany 24th – 26th September, VDI Berichte 1685, VDI/VDE-Gesellschaft Mess- und Automatisierungstechnik*

[46] Pratt J R, Kramar J A, Shaw G, Gates R, Rice P, Moreland J 2006 New reference standards and artifacts for nanoscale property characterization *Proc. 11th NSTI Nanotech, Boston, USA, 1st – 5th June*

[47] Villanueva G 2006 Piezoresistive cantilevers in a commercial CMOS technology for intermolecular force detection *Microelectronic Engineering* **83** 1302–1305

[48] Kumar V V, Dasgupta A, Bhat K N 2006 Process optimization for monolithic integration of piezoresistive pressure sensor and MOSFET amplifier with SOI approach *J. Phys.: Conf. Ser.* **34** 210–215

[49] Cumpson P J, Hedley J, Clifford C A 2005 Microelectromechanical device for lateral force calibration in the atomic force microscope: Lateral electrical nanobalance *J. Vac. Sci. Technol. B* **23** 1992–1997

[50] Leach R K, Flack D R, Hughes E B, Jones C W 2007 Development of a new traceable areal surface texture measuring instrument *Proc. 11th Int. Conf. Metrology & Properties of Engineering Surfaces, Huddersfield, UK, 17th – 20th July* 64–68

[51] Mohanty P, Harrington D A, Ekinci K L, Yang Y T, Murphy M J, Roukes M L 2002 Intrinsic dissipation in high-frequency micromechanical resonators *Phys. Rev. B* **66** 085416

[52] Keely C A 1989 Solder joint inspection using laser Doppler vibrometry *Hewlett-Packard Journal, October* 81-85

[53] Stalder A, Dürig U 1995 Nanoguitar: Oscillating string as force sensor *Rev. Sci. Instrum.* **66** 3576–3579

[54] Fukuzawa K, Ando T, Shibamoto M, Mitsuya Y, Zhang H 2006 Monolithically fabricated double-ended tuning-fork-based force sensor *J. Appl. Phys.* **99** 094901

[55] Sato K, Ono A, Tomikawa Y 2003 Finite element method simulation of double-ended tuning-fork quartz resonator for application to vibratory gyro-sensor *Jpn. J. Appl. Phys.* **42** 3115–3119

[56] Harley J A, Kenny T W 2001 A high-stiffness axial resonant probe for atomic force microscopy *J. Microelectromechanical Systems* **10** 434–441.

[57] Sazonova V, Yaish Y, Üstünel H, Roundy D, Arias T A, McEuen P L 2004 A tunable carbon nanotube electromechanical oscillator *Nature* **431** 284–287

[58] Autumn K, Sitti M, Liang Y A, Peattie A M, Hansen W R, Sponberg S, Kenny T W, Fearing R, Israelachvili J N, Full R J 2002 Evidence for van der Waals adhesion in gecko setae *PNAS* **99** 12252

[59] Argento C, French R H 1996 Parametric tip model and force-distance relation for Hamaker constant determination from atomic force microscopy *J. Appl. Phys.* **80** 6081–6090

[60] Ackler H D, Frend R H, Chiang Y-M 1996 Comparisons of Hamaker constants for ceramic systems with intervening vacuum or water: from force laws and physical properties *J. Colloid Interface Sci.* **179** 460–469

[61] Lamoreaux S K 1997 Demonstration of the Casimir force in the 0.6 to 6 μm range *Phys. Rev. Lett.* **78** 5–8

[62] Mohideen U, Roy A 1998 Precision measurement of the Casimir force from 0.1 to 0.9 μm *Phys. Rev. Lett.* **81** 4549–4552

[63] Bulgac A, Magierski P, Wirzba A 2006 Scalable Casimir effect between Dirichlet spheres or a plate and a sphere *Phys. Rev. D* **73** 025007

[64] Sparnaay M J 1958 Measurement of attractive forces between flat plates *Physica* **24** 751–764

[65] Choi J-H, Kim M-S, Park Y-K 2007 Quantum-based mechanical force realization in the piconewton range *Appl. Phys. Lett.* **90** 073117

[66] Carrion-Vazquez M, Oberhauser A F, Fowler S B, Marszalek P E, Broedel S E, Clarke J, Fernandez J M 1999 Mechanical and chemical unfolding of a single protein: A comparison *PNAS* **96** 3694–3699

[67] Oberhauser A, Hansma P, Carrion-Vazquez M, Fernandez J M 2001 Stepwise unfolding of titin under force-clamp atomic force microscopy *PNAS* **98** 468–472

[68] Oberhauser A F, Marszalek P E, Erickson H P, Fernandez J M 1998 The molecular elasticity of the extracellular matrix protein tenascin *Nature* **393** 181–185

[69] Fulton A, Isaacs W 1991 Titin, a huge, elastic sarcomeric protein with a probable role in morphogenesis *Bioessays* **13** 157–161

[70] Rief M, Gautel M, Oesterhelt, Fernandez J M, Gaub H E 1997 Reversible unfolding of individual titin immunoglobulin domains by AFM *Science* **276** 1109–1112

[71] Gao M, Lu H, Schulten K 2001 Simulated refolding of stretched titin immunoglobulin domains *Biophysical Journal* **81** 2268–2277

[72] Marszalek P E, Oberhauser A F, Pang Y P, Fernandez J M 1998 Polysaccharide elasticity governed by chair±boat transitions of the glucopyranose ring *Nature* **396** 661–664

[73] Wright W M D, Chetwynd D G 1998 Can charge writing aid nanotechnological manipulation? *Nanotechnology* **9** 133–142

[74] Degertekin F L, Hadimioglu B, Sulchek T, Quate C F 2001 Actuation and characterization of atomic force microscope cantilevers in fluids by acoustic radiation pressure *Appl. Phys. Lett.* **78** 1628–1630

[75] Dushkin C D, Yoshimura H, Nagayama K 1996 Note – Direct measurement of nanonewton capillary forces *Journal of Colloid and Interface Science* **181** 657–660

[76] Young H D, Freedman R A 2000 *University physics with modern physics* (Tenth Edition, Addison-Wesley)

[77] Sitti M, Hashimoto H 2000 Controlled pushing of nanoparticles: modelling and experiments *IEEE/ASME Trans. Mechatronics* **5** 199-211

[78] Burnham N A, Colton R J, Pollock H M 1993 Interpretation of force curves in force microscopy *Nanotechnology* **4** 64–80

[79] Tabor D 1991 *Gases, liquids and solids; and other states of matter* (Cambridge University Press: Cambridge)